Photophysics

Deutsche Ausgabe: DOI: 10.1002/ange.201509798
Internationale Ausgabe: DOI: 10.1002/anie.201509798

# Near-IR Emitting Iridium(III) Complexes with Heteroaromatic β-Diketonate Ancillary Ligands for Efficient Solution-Processed OLEDs: Structure–Property Correlations

*Sagar Kesarkar, Wojciech Mróz, Marta Penconi, Mariacecilia Pasini, Silvia Destri, Marco Cazzaniga, Davide Ceresoli, Patrizia R. Mussini, Clara Baldoli, Umberto Giovanella,* and Alberto Bossi**

***Abstract:*** *Three NIR-emitting neutral $Ir^{III}$ complexes [Ir(iqbt)$_2$(dpm)] (**1**), [Ir(iqbt)$_2$(tta)] (**2**), and [Ir(iqbt)$_2$(dtdk)] (**3**) based on the 1-(benzo[b]thiophen-2-yl)-isoquinolinate (iqtb) were synthesized and characterized (dpm = 2,2,6,6-tetramethyl-3,5-heptanedionate; tta = 2-thienoyltrifluoroacetonate; dtdk = 1,3-di(thiophen-2-yl)propane-1,3-dionate). The compounds emit between λ = 680 and 850 nm with high luminescence quantum yields (up to 16 %). By combining electrochemistry, photophysical measurements, and computational modelling, the relationship between the structure, energy levels, and properties were investigated. NIR-emitting, solution-processed phosphorescent organic light-emitting devices (PHOLEDs) were fabricated using the complexes. The devices show remarkable external quantum efficiencies (above 3 % with **1**) with negligible efficiency roll-off values, exceeding the highest reported values for solution-processible NIR emitters.*

Driven by military,[1] civil, and telecommunications needs, the development of near-IR-emissive materials (emitting at wavelengths greater than λ = 700 nm) has emerged as a promising and challenging research field with potential application in organic light emitting diodes (OLEDs), night-vision readable displays, and bio-imaging.[1,2]

NIR emitters suitable for OLED application have been developed either using pure organic molecules and/or polymers or organometallic compounds.[3] Late-transition-metal complexes of the second and third row display high luminescence quantum efficiencies ($\Phi_L$) resulting from strong spin-orbit coupling (a result of the heavy metal effect) and intrinsic conformational rigidity. In addition, the ease of engineering their electronic properties make these compounds of particular relevance in NIR applications.[4] Phosphorescent OLEDs (PHOLEDs), in which both singlet and triplet excitons can be harvested,[5] have shown record external quantum efficiencies (EQE) of 9–14.5 % in the λ = 650–800 nm range employing Pt porphyrins or excimeric Pt compounds in sophisticated device architectures.[6] However, detrimental efficiency roll-off at increasing current density was detected.[5a,7] This effect is primarily ascribed to the facile aggregation of square-planar systems and their intrinsic long phosphorescence lifetimes. On the other hand, phosphorescent cyclometalated transition-metal complexes with octahedral geometries (containing, for example, $Ir^{III}$,[8a,b] $Os^{II}$,[8c] or $Re^{I}$[8d]) have been also been explored to limit the efficiency roll-off issues.

Cao et al. reported an iridium(III)-based solution-processed optimized device with an emission maximum at λ = 690 nm and an EQE value over 5 %.[9] Similarly, Tao et al. demonstrated negligible efficiency roll-off in $Ir^{III}$-based devices, obtained by solution or vacuum methods, emitting in the range λ = 700–800 nm with EQE values of about 2 %.[10]

The most successful strategy to lower the emission energy of cyclometalated complexes, based on the use of a chelating ligand with *N^C* donor atoms,[3c] is the careful expansion of the π conjugation of the ligand system.[11–13] For instance, a red shift of over 100 nm can be achieved employing isoquinoline and naphthyl groups instead of pyridine and phenyl rings.[14,15] Additionally, introducing electron-rich heteroaromatic rings (such as thiophene) also induces a significant bathochromic shift in the emission.[16] Alternatively, significant electronic perturbation can be achieved by modification of the ancillary ligands.[17] The introduction of β-diketonate ancillary ligands onto homoleptic tris-cyclometalated $Ir^{III}$ complexes can induce a slight red shift (10–15 nm) of the emission as in the case of [Ir(thpy)$_2$(acac)] and [Ir(btpy)$_2$(acac)] compared to *fac*-[Ir(thpy)$_3$] and *fac*-[Ir(btpy)$_3$], respectively (thpy = 2-thienylpyridine; btpy = benzothienylpyridine; acac = acetylacetonate).[18]

Ikawa et al. recently reported a homoleptic *fac*-[Ir(iqbt)$_3$] complex (iqbt = 1-(benzo[*b*]thiophen-2-yl)-isoquinoline), incorporating electron-rich benzothiophene moieties, which emits at λ = 690 nm with good efficiency.[19] A solution-processed OLED incorporating this complex was fabricated with an EQE of 1.4 %.[19a]

We decided to investigate the family of [Ir(iqbt)$_2$L] complexes including three different β-diketonate (L) ancillary ligands with increasing conjugation. The three ancillary ligands employed were 2,2,6,6-tetramethyl-3,5-heptanedione

[*] Dr. S. Kesarkar, Dr. M. Penconi, Dr. M. Cazzaniga, Dr. D. Ceresoli, Dr. C. Baldoli, Dr. A. Bossi
Istituto di Scienze e Tecnologie Molecolari–CNR and SmartMatLab Center, Via C. Golgi 19, 20133 Milano (Italy)
E-mail: alberto.bossi@istm.cnr.it
Dr. W. Mróz, Dr. M. Pasini, Dr. S. Destri, Dr. U. Giovanella
Istituto per lo Studio delle Macromolecole–CNR
Via E. Bassini 15, 20133 Milano (Italy)
E-mail: u.giovanella@ismac.cnr.it
Prof. P. R. Mussini
Dipartimento di Chimica, Università degli Studi di Milano
Via Golgi 19, 20133 Milano (Italy)
Supporting information and ORCID(s) from the author(s) for this article are available on the WWW under http://dx.doi.org/10.1002/anie.201509798.

  

(Hdpm), 2-thienoyltrifluoroacetone (Htta) featuring one thiophene group, and 1,3-di(thiophen-2-yl)propane-1,3-dione (Hdtdk) featuring two thiophene groups. These three ligands allowed control of the steric hindrance and solubility of the complexes (critical for processing of the active layer of the devices) and have increased donor character because of the presence of the electron-rich thiophene groups. Moreover, the possibility of selective functionalization of the thiophene ring in the tta and dtdk ligands makes these derivatives even more attractive. With this simple strategy, we synthesized three new NIR-emitting $Ir^{III}$ complexes which were employed to prepare efficient PHOLEDs having negligible efficiency roll-off values in unoptimized devices.

The new complexes, **1**–**3** (Figure 1) were prepared using a two-step process (see Scheme S1.2 in the Supporting Information). The intermediate μ-chloro-bridged dimer, $[\{(iqbt)_2IrCl\}_2]$, prepared by cyclometalation of $IrCl_3 \cdot n H_2O$ with the Hiqbt ligand,[20a] was reacted with Hdpm in 2-ethoxyethanol as solvent at 110 °C in the presence of $K_2CO_3$ to give **1** in 22 % yield.[20b] A slight modification of this procedure was needed for the synthesis of **2** and **3** which were obtained in 32 % and 24 % yield, respectively (see the Supporting Information).[20c] All complexes are soluble in common organic solvents.

The UV/Vis/NIR absorption spectra of the three complexes in $CH_2Cl_2$ at 298 K (Table 1 and Figure 2a) show strong absorption bands in the region below $\lambda = 450$ nm; this results from a complex spectroscopic admixture of π–π* and metal-to-ligand charge transfer (MLCT) transitions.[21]

Complexes **2** and **3**, compared to **1**, show larger extinction coefficients ($\varepsilon$) in the range $\lambda = 350$–400 nm because of the overlap of the original diketonate ligand (Hdtdk and Htta) absorption bands.[22] In the region $\lambda = 450$–600 nm the absorption shape of **1**, **2**, and **3** is similar and undergoes a blue shift in the sequence **1**, **3**, **2**. Since the ligands (iqbt and diketonates) do not absorb in that region, we assign these bands to $^{1,3}$MLCT (d–π*) transitions resulting from the coordination of the $Ir^{III}$ center with the iqbt ligand. Weak bands in the region of $\lambda > 600$ nm (Figure 2a, inset) are assigned to ground-state excitation into the lowest triplet state ($S_0 \rightarrow T_1$; Table 1 and see below for TDDFT analysis).[16]

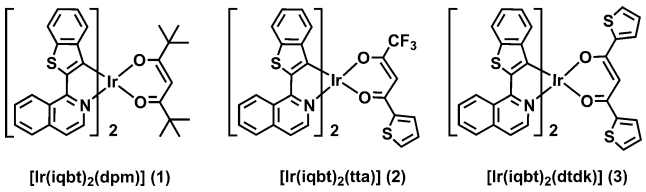


***Figure 1.*** Chemical structures of complexes **1**–**3**.

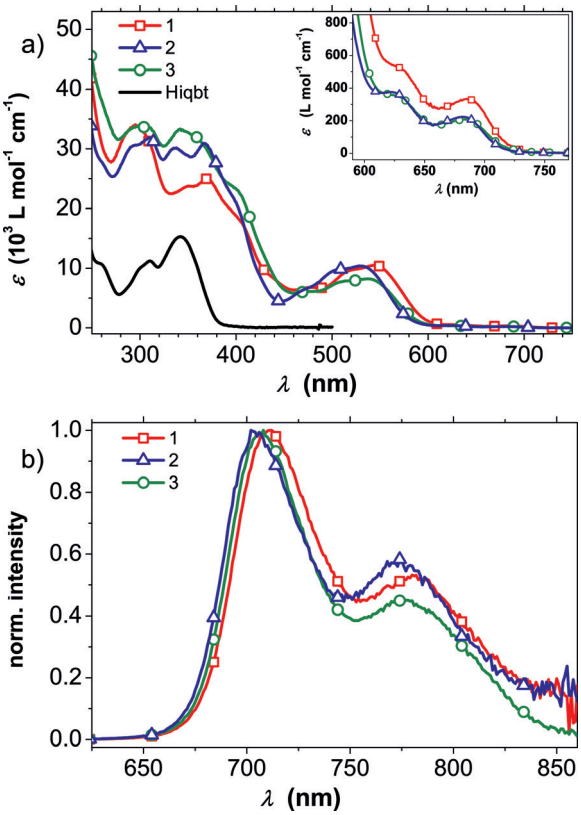


***Figure 2.*** a) UV/Vis/NIR absorption and b) emission spectra in $CH_2Cl_2$ at 298 K of **1** (red), **2** (blue), and **3** (green). In (a), the spectrum of the Hiqbt ligand is shown for comparison (black). Inset in (a): the $S_0$–$T_1$ absorption bands.

Complexes **1**, **2**, and **3** display a structured NIR phosphorescence emission at $\lambda = 710$, 704, and 707 nm, respectively, recorded at 298 K in degassed $CH_2Cl_2$ solution (Table 1 and Figure 2b). As a result of the nonemissive character of the dpm ligand and the high triplet energy ($E_T$) of ligands dtdk and tta (emission maxima at $\lambda = 531$ nm and 502 nm)[16] compared to Hiqbt ($\lambda = 580$ nm; Figure S2.5), the emissions

***Table 1:*** Photophysical properties of complexes **1**–**3**.

| | Absorption[a] | | Emission 298 K[a] | | | | | Emission 77 K[c] | | Electrochemistry[d] | | |
|---|---|---|---|---|---|---|---|---|---|---|---|---|
| | $\lambda_{abs}$ [nm] ($\varepsilon$ [$\times 10^3$ L mol$^{-1}$ cm$^{-1}$]) | $E_g^{OPT}$[b] [eV] | $\lambda_{em}$ [nm] | $\tau$ [μs] | $\Phi_L$ | $k_r$ [$\times 10^5$ s$^{-1}$] | $k_{nr}$ [$\times 10^5$ s$^{-1}$] | $\lambda_{em}$ [nm] | $\tau$ [μs] | HOMO [eV] | LUMO [eV] | $E_g^{EC}$ [eV] |
| **1** | 545 (10.5) (MLCT)<br>687 (0.34) ($S_0$–$T_1$) | 2.27 | 710 | 1.40 | 0.16 | 1.1 | 6.0 | 694 | 2.04 | −5.15 | −2.71 | 2.44<br>(2.29)[e] |
| **2** | 528 (10.4) (MLCT)<br>681 (0.23) ($S_0$–$T_1$) | 2.35 | 704 | 0.72 | 0.07 | 0.97 | 13.0 | 691 | 2.03 | −5.31 | −2.96 | 2.35<br>(2.07)[e] |
| **3** | 539 (8.2) (MLCT)<br>687 (0.21) ($S_0$–$T_1$) | 2.30 | 707 | 1.44 | 0.14 | 0.97 | 6.0 | 694 | 2.00 | −5.19 | −2.76 | 2.43<br>(2.25)[e] |

[a] $N_2$-saturated $CH_2Cl_2$ solutions ($c_M \approx 2 \times 10^{-5}$ L mol$^{-1}$) at 298 K. Absorption maxima at wavelengths greater than $\lambda = 500$ nm given. Rate constants $k_r$ and $k_{nr}$ are calculated using the equations $k_r = \Phi_L/\tau$ and $k_{nr} = (1-\Phi_L)/\tau$, on the assumption that $\Phi_{ISC} = 1$ (ISC = intersystem crossing). [b] Calcd. at $\lambda_{abs,MLCT}$. [c] In a 2-MeTHF frozen matrix at 77 K. [d] Calcd. from $E^0$ potentials. [e] Calcd. from onset criterion (Table S3).

  

of **1–3** originate from a perturbed iqbt-based state with $^3$LC/$^3$MLCT character (LC = ligand-centered; see Figure 4 for the DFT calculations and Section S4 in the Supporting Information). Although the phosphorescence emission of complexes **1–3** shifts slightly to mirror the absorption behavior, the excited-state dynamics of the complexes are clearly affected by the diketonate structure. Complexes **1** and **3** show almost identical luminescence quantum yields $\Phi_L$ (0.16 and 0.14, respectively) and lifetimes (1.40 μs and 1.44 μs), whereas a two-fold decrease is detected for **2** ($\Phi_L = 0.07$ and $\tau = 0.72$ μs). Radiative rate constants ($k_r$) are high and are essentially identical for the three complexes (circa $1 \times 10^5$ s$^{-1}$ in accordance with the large $\varepsilon$ value of the $S_0 \rightarrow T_1$ transition) whereas the nonradiative rate ($k_{nr}$) for **2** is two times larger than those for **1** and **3**. A minor rigidochromic blue shift is detected at 77 K in a 2-MeTHF matrix (Figure S2.6; Table 1) and the excited-state lifetimes increase up to about 2 μs for all of the complexes. This evidence suggests the presence of a competitive, thermally activated (TA), nonradiative deactivation pathway in **2** that sidesteps the vibrational coupling pathway to the ground state also present in **1** and **3**.

To further investigate the nature of shift of the $^{1,3}$MLCT bands and the different decay dynamics, we performed electrochemical studies and determined the frontier orbital energy levels. These data were further used in the choice of OLED host materials. In the cyclic voltammograms, a reversible oxidation wave is detected at +0.38 V, +0.54 V and +0.43 V versus $Fc^+$/Fc for **1**, **2**, and **3**, respectively (Figure 3; Figure S3.1), attributed to a predominantly metal-centered process also involving the cyclometalated benzothiophene moiety,[23] as evidenced by the DFT calculations (Figure 4; Figure S4.1).

The anodic shift in oxidation (HOMO level stabilization) of **3** (0.05 eV) compared to **1** may result from the larger π-backbonding from the $Ir^{III}$ center to the dtdk ligand resulting from the more extended conjugation of the diketonate ligand itself.[24] In comparison to **1**, the stronger anodic shift of **2** (0.16 eV) results from the combined effects of π-backbonding (in analogy to **3**) enhanced by the electron-withdrawing effect of the $CF_3$ group on the tta moiety. No further oxidation is detected for **1**, whereas a second irreversible oxidation wave at +0.92 V for **3** and at +1.02 V for **2** is assigned to electrochemical processes on the thiophene unit of the diketonate ligand.

Two reversible reduction waves are detected for **1** at −2.12 V and −2.43 V, and can be attributed to two subsequent one-electron reduction processes localized on the isoquinoline moiety.[25] Complexes **2** and **3** show three reduction waves. The first one-electron reversible reduction wave is located at −1.87 V for **2** and −2.07 V for **3**, anodically shifted compared to **1** by 0.25 V and 0.05 V, respectively. The next two, quasi-reversible, reduction processes are detected below −2.3 V. Thus, the electrochemical HOMO–LUMO gaps ($E_g^{EC}$) follows the order **2** < **3** < **1**, contrary to the detected optical gap ($E_g^{OPT}$ are ordered **1** < **3** < **2**).

In contrast, the same energy trends are found comparing $E_g^{OPT}$ and $E_g^{EC}$ gap values for **2** and **3** calculated between the first oxidation and second reduction waves (Table S3.1), suggesting that the first reduction process would involve orbitals on the diketonate dtdk and tta ligands.[26]

In agreement with this conclusion, DFT calculations show a large LUMO density distribution on the diketonate ligand in case **2** and **3** in contrast to the iqbt-localized LUMO in **1** (Figure 4; Figure S4.1). Thus, the next two cathodic reduction waves of **2** and **3** are attributed to iqbt-localized processes; compared to the analogous processes in **1**, their cathodic potentials shift (level destabilization) indicates a partial electronic communication between the LUMO and the adjacent LUMO + 1 and LUMO + 2 orbitals. Pictorially we observe the LUMO + 1 density spreading onto the iqbt ligand but also onto the tta/dtdk ligands in **2** and **3**.[25]

Time-dependent DFT (TDDFT) calculations were performed to further confirm the nature of the electronic transitions described (simulated spectra are reported in Figure S4.3 and Table S4.1 summarize the main transitions and the orbital analyses).

The calculated lowest energy triplet transitions ($S_0$–$T_1$) are in the range $\lambda = 724$–718 nm following the experimental trend. In **1**, the lowest energy singlet transitions ($\lambda = 557$ and 545 nm) share a HOMO–LUMO and HOMO–LUMO +

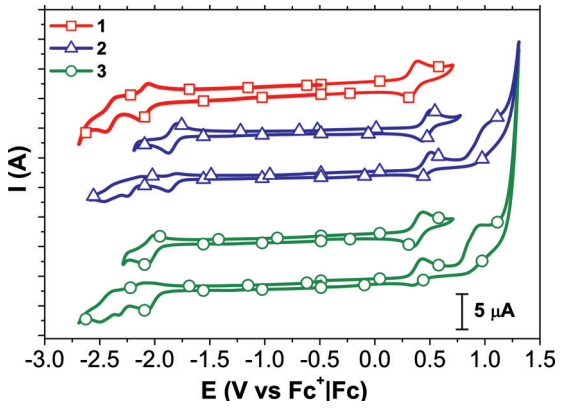


***Figure 3.*** Cyclic voltammograms of complexes **1–3** recorded versus $Fc^+$/Fc in DMF at 298 K under a $N_2$ atmosphere (scan rate = 100 mV s$^{-1}$).

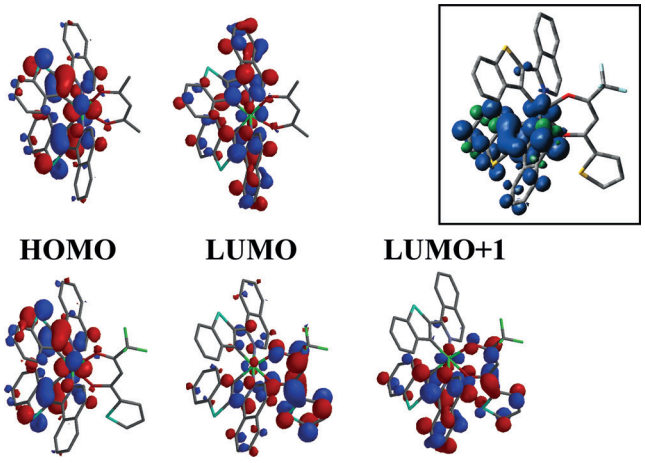


***Figure 4.*** DFT B3LYP/LACVP** frontier orbital counterplots (optimized ground state) of **1** (top) and **2** (bottom) and triplet spin density of **2** (boxed) in the optimized triplet state.

1 character. In agreement with the absorption trend, a hypsochromic shift to 537 nm in **2** and to 543 nm in **3** is detected and, in contrast to **1**, these transitions arise from HOMO to LUMO + 2 transitions.

Within this energetic framework, the nonradiative TA path that quenches the emission of **2** could involve population of a low-lying metal-ligand-to-ligand CT state of HOMO to LUMO character which (according to the CV onset gap of 2.07 eV) sits only 0.25 eV above the emissive $^3$LC/$^3$MLCT state (at 1.79 eV, equivalent to an emission peak at $\lambda =$ 691 nm).

Further confirmation arises from TDDFT calculations in which, for both **2** and **3**, a weak singlet transition from the HOMO to the LUMO is found (occurring at $\lambda = 586$ nm and 572 nm, respectively), emphasizing the importance of the shift of the LUMO onto the tta/dtdk ligands. Therefore the smaller calculated singlet–triplet gap in **2** and **3** compared to **1** would justify the higher quenching rate which is detected at least in **2**.

The novel soluble NIR emitters were tested in solution-processed devices with a simple architecture of ITO/PEDOT:PSS(50 nm)/PVK(65 %):OXD7(30 %):Ir complex-(5 %)(180 nm)/Ba(7 nm)/Al(100 nm) (ITO = indium tin oxide; PEDOT:PSS = poly(3,4-ethylenedioxythiophene) polystyrene sulfonate; OXD7 = 1,3-bis(5-(4-*tert*-butylphenyl)-1,3,4-oxadiazol-2-yl)benzene; PVK = polyvinylcarbazole).[27] Thanks to the suitable choice of PVK as host, efficient emission in the spectral range $\lambda = 680$–900 nm is detected for all the devices.

Electroluminescence (EL) spectra (Figure 5 a) resemble very well those recorded for the complexes in $CH_2Cl_2$ (Figure 2 b), with emission maxima at $\lambda = 714$ nm for **1** and **3** and $\lambda = 709$ nm for **2** and negligible contribution from the matrix. However, emission spectra (Figure S5.3) of the devices reveal a weak PVK contribution at $\lambda = 420$ nm, suggesting that a charge-trapping mechanism is responsible for the EL, facilitated by the position of the HOMO and LUMO levels of the emitters with respect to the matrix energy levels (Figure 5 a, inset).

The PHOLED based on **1** shows a remarkable total EQE ($EQE_{tot}^{max}$) of 3.07 % at 1 mA cm$^{-2}$. For **3** and **2** the efficiencies are 2.44 % and 1.28 %, respectively, mirroring the $\Phi_L$ trend in solution. The devices switch on at 13–15 V (Figure S 5.1) and the EQE values remain indeed constant in the radiance ($L_e$) range 0.1–1 W sr$^{-1}$ m$^{-2}$ (Table 2; Figure 5 b).

Therefore, the device efficiency roll-off at high brightness, ascribed to triplet–triplet annihilation or triplet–polaron quenching,[28] is negligible for emitters **1** and **3** and only moderate (about 10 %) for **2**, resulting from the short radiative lifetimes and reduced aggregation of the complexes. In complex **2**, electron-trapping on the lower-energy LUMO could lead to a decreased EQE value.

In conclusion, we prepared three cyclometalated Ir$^{III}$ complexes with different β-diketonate ancillary ligands which demonstrate efficient NIR emission. Electrochemical and photophysical studies, supported by DFT calculations, allowed correlation of the structure–property effects as a consequence of changing LUMO energies with modification of the diketonate structure. Unoptimized devices were fabricated to test the effect of changing the nature of the ligand on the optoelectronic properties. The PHOLED based on emitter **1** showed a remarkable EQE of 3.07 %, in a single layer architecture and with negligible efficiency roll-off, which is a key feature for technological applications. These devices rank among the most efficient devices reported employing a true NIR-emitting phosphorescent complex.

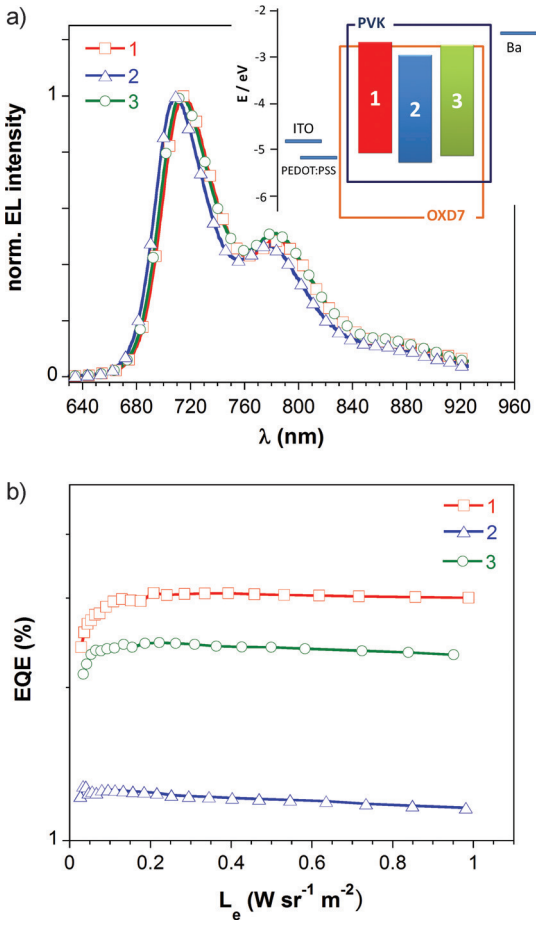


***Figure 5.*** a) EL spectra and b) EQE versus radiance plots (bottom) for PHOLEDs based on complexes **1**–**3**. Inset in (a): Flat-band energy level diagram for the devices.

***Table 2:*** Characteristics of the devices based on **1**–**3**.[a]

| | $\lambda_{max}^{EL}$ [nm] | *d* [nm] | $V_{on}$ [V] | $EQE_{tot}^{max}$ [%] | $L_e^{max}$ [W sr$^{-1}$ m$^{-2}$] |
|---|---|---|---|---|---|
| **1** | 714 | 233 | 13 | 3.07 | 1.43 |
| **2** | 709 | 235 | 15 | 1.28 | 3.1 |
| **3** | 714 | 234 | 14 | 2.44 | 4.9 |

[a] Von is the turn-on voltage; *d* is the total thickness of the organic layers.

## Acknowledgements

We thank Regione Lombardia (grant number 3667/2013; project TIMES "Tecnologie e materiali per l'utilizzo efficiente dell'energia solare") and Progetto Integrato Regione

  

Lombardia and Fondazione CARIPLO (grant numbers 12689/13, 7959/13; Azione 1 e 2, "SmartMatLab centre") for financial support. The authors acknowledge Dr. Fausto Cargnoni for useful discussions on TDDFT experiments.

**Keywords:** density functional calculations · electrochemistry · iridium · organic light emitting diodes · phosphorescence

**How to cite:** *Angew. Chem. Int. Ed.* **2016**, *55*, 2714–2718
*Angew. Chem.* **2016**, *128*, 2764–2768

[1] J. Heerlein, M. Behringer, C. Jäger, "Near-infrared power LED for emerging security and defence applications", *Proc. SPIE* 8186, Electro-Optical Remote Sensing, Photonic Technologies, and Applications V, 81860O (October 05, **2011**); DOI: 10.1117/12.897992.

[2] a) G. Qian, Z. Y. Wang, *Chem. Asian J.* **2010**, *5*, 1006–1029; b) H. Xu, R. Chen, Q. Sun, W. Lai, Q. Su, W. Huang, X. Liu, *Chem. Soc. Rev.* **2014**, *43*, 3259–3302.

[3] a) J. Kido, *Chem. Rev.* **2002**, *102*, 2357–2368; b) T. T. Steckler, O. Fenwick, T. Lockwood, M. R. Andersson, F. Cacialli, *Macromol. Rapid Commun.* **2013**, *34*, 990–996; c) H. Xiang, J. Cheng, X. Ma, X. Zhou, J. J. Chruma, *Chem. Soc. Rev.* **2013**, *42*, 6128–6185.

[4] W. Y. Wong, *Organometallics and Related Molecules for Energy Conversion, Green Chemistry and Sustainable Technology* (Ed.: W. Y. Wong), Springer, Heidelberg, **2015**.

[5] a) M. A. Baldo, D. F. O'Brien, Y. You, A. Shoustikov, S. Sibley, M. E. Thompson, S. R. Forrest, *Nature* **1998**, *395*, 151–154; b) Y. Sun, N. C. Giebink, H. Kanno, B. Ma, M. E. Thompson, S. R. Forrest, *Nature* **2006**, *440*, 908–912.

[6] a) K. R. Graham, Y. Yang, J. R. Sommer, A. H. Shelton, K. S. Schanze, J. Xue, J. R. Reynolds, *Chem. Mater.* **2011**, *23*, 5305–5312; b) J. Kalinowski, V. Fattori, M. Cocchi, J. A. G. Williams, *Coord. Chem. Rev.* **2011**, *255*, 2401–2425, and Ref. [87] therein.

[7] C. Murawaski, K. Leo, M. C. Gather, *Adv. Mater.* **2013**, *25*, 6801–6868.

[8] a) Q. L. Xu, X. Liang, S. Zhang, Y. M. Jing, X. Liu, G. Z. Lu, Y. X. Zheng, J. L. Zuo, *J. Mater. Chem. C* **2015**, *3*, 3694–3701; b) L. Han, D. Zhang, J. Wang, Z. Lan, R. Yang, *Dyes Pigm.* **2015**, *113*, 649–654; c) C. Lee, J. Y. Hung, Y. Chi, Y. M. Cheng, G. H. Lee, P. T. Chou, C. C. Chen, C. H. Chang, C. C. Wu, *Adv. Funct. Mater.* **2009**, *19*, 2639–2647; d) X. Li, D. Zhang, H. Chi, G. Xiao, Y. Dong, S. Wu, Z. Su, Z. Zhang, P. Lei, Z. Hu, W. Li, *Appl. Phys. Lett.* **2010**, *97*, 263303.

[9] X. Cao, J. Miao, M. Zhu, C. Zhong, C. Yang, H. Wu, J. Qin, Y. Cao, *Chem. Mater.* **2015**, *27*, 96–104.

[10] a) R. Tao, J. Qiao, G. Zhang, L. Duan, C. Chen, L. Wang, Y. Qiu, *J. Mater. Chem. C* **2013**, *1*, 6446–6454; b) R. Tao, J. Qiao, G. Zhang, L. Duan, L. Wang, Y. Qiu, *J. Phys. Chem. C* **2012**, *116*, 11658–11664.

[11] M. E. Thompson, P. I. Djurovich, S. Barlow, S. R. Marder in *Comprehensive Organometallic Chemistry*, *Vol. 12* (Ed.: D. O'Hare), Elsevier, Oxford, **2007**, pp. 101–194.

[12] A. Bossi, A. F. Rausch, M. Leitl, R. Czerwieniec, M. T. Whited, P. I. Djurovich, H. Yersin, M. E. Thompson, *Inorg. Chem.* **2013**, *52*, 12403–12415.

[13] C.-L. Ho, H. Li, W.-Y. Wong, *J. Organomet. Chem.* **2014**, *751*, 261–285.

[14] J. Brooks, Y. Babayan, S. Lamansky, P. I. Djurovich, I. Tsyba, R. Bau, M. E. Thompson, *Inorg. Chem.* **2002**, *41*, 3055–3066.

[15] H. Yersin in *Highly Efficient OLEDs with Phosphorescent Materials* (Ed.: H. Yersin), Wiley-VCH, Weinheim, **2007**.

[16] W. J. Finkenzeller, T. Hofbeck, M. E. Thompson, H. Yersin, *Inorg. Chem.* **2007**, *46*, 5076–5083.

[17] B. J. Powell, *Coord. Chem. Rev.* **2015**, *295*, 46–79.

[18] a) A. Tsuboyama, H. Iwawaki, M. Furugori, T. Mukaide, J, Kamatani, S. Igawa, T. Moriyama, S. Miura, T. Takiguchi, S. Okada, M. Hoshino, K. Ueno, *J. Am. Chem. Soc.* **2003**, *125*, 12971–12979; b) S. Lamansky, P. Djurovich, D. Murphy, F. Abdel-Razzaq, H.-E. Lee, C. Adachi, P. E. Burrows, S. R. Forrest, M. E. Thompson, *J. Am. Chem. Soc.* **2001**, *123*, 4304–4312.

[19] a) S. Ikawa, S. Yagi, T. Maeda, H. Nakazumi, H. Fujiwara, S. Koseki, Y. Sakurai, *Inorg. Chem. Commun.* **2013**, *16*, 14–19; b) "Compound and functional luminescent probe comprising the same": S. Tobita, T. Yoshihara, M. Hosaka, T. Takeuchi, Patent number US 8,623,239 B2, **2014**.

[20] a) M. Nonoyama, *Bull. Chem. Soc. Jpn.* **1974**, *47*, 767–768; b) S. Lamansky, P. Djurovich, D. Murphy, F. Abdel-Razzaq, R. Kwong, I. Tsyba, M. Bortz, B. Mui, R. Bau, M. E. Thompson, *Inorg. Chem.* **2001**, *40*, 1704–1711; c) T. Yu, S. Yang, J. Meng, Y. Zhao, H. Zhang, D. Fan, X. Han, Z. Liu, *Inorg. Chem. Commun.* **2011**, *14*, 159–161.

[21] G.-N. Li, Y. Zou, Y.-D. Yang, J. Liang, F. Cui, T. Zheng, H. Xie, Z.-G. Niu, *J. Fluoresc.* **2014**, *24*, 1545–1552.

[22] C. Freund, W. Porzio, U. Giovanella, F. Vignali, M. Pasini, S. Destri, A. Mech, S. Di Pietro, L. Di Bari, P. Mineo, *Inorg. Chem.* **2011**, *50*, 5417–5429.

[23] K. R. J. Thomas, M. Velusamy, J. T. Lin, C. H. Chien, Y. T. Tao, Y. S. Wen, Y. H. Hu, P. T. Chou, *Inorg. Chem.* **2005**, *44*, 5677–5685.

[24] M. K. Nazeeruddin, R. Humphry-Baker, D. Berner, S. Rivier, L. Zuppiroli, M. Graetzel, *J. Am. Chem. Soc.* **2003**, *125*, 8790–8797.

[25] S. Ikawa, S. Yagi, T. Maeda, H. Nakazumi, H. Fujiwara, S. Koseki, Y. Sakurai, *Inorg. Chem. Commun.* **2013**, *16*, 14–19.

[26] K. Beydoun, M. Zaarour, J. A. G. Williams, T. Roisnel, V. Dorcet, A. Planchat, A. Boucekkine, D. Jacquemin, H. Doucet, V. Guerchais, *Inorg. Chem.* **2013**, *52*, 12416–12428.

[27] OXD7 was used as an additive to improve charge balance within the emissive layer. See, for example: W. Mróz, R. Ragni, F. Galeotti, E. Mesto, C. Botta, L. De Cola, G. M. Farinola, U. Giovanella, *J. Mater. Chem. C* **2015**, *3*, 7506–7512.

[28] S. Reineke, K. Walzer, K. Leo, *Phys. Rev. B* **2007**, *75*, 125328.

Received: October 19, 2015
Revised: December 16, 2015
Published online: January 25, 2016

  